

MODELLING OF PATTERN FORMATION DURING THE MELTING OF SILICON BY A HF EM FIELD

K. Bergfelds, J. Virbulis, A. Krauze

*Faculty of Physics and Mathematics, University of Latvia,
8 Zella str., LV-1002, Riga, Latvia
e-Mail: janis.virbulis@lu.lv*

The present work investigates reasons of inhomogeneous silicon melting in floating-zone crystal growth. It is proposed that this phenomenon is caused by the concentration of electric current in the melt induced by different material properties of the silicon melt and the solid. A coupled model of electromagnetic, temperature and phase change fields has been developed and used to describe the transient melting-solidification process. The Octave/Matlab script language is used for the implementation of this model. Calculation results demonstrate that the melt structure development is related to the magnetic skin-depth in solid silicon.

Introduction. In the floating-zone (FZ) crystal growth, a high-frequency electromagnetic (HF EM) field is used to melt a polycrystalline silicon (Si) feed rod. Usually an inductor current with a frequency of around 3 MHz is used to ensure a sufficiently small penetration depth of the EM field for proper melting of the feed rod [1]. In case of lower frequencies, the melting surface of the feed rod can give rise to instabilities [2].

However, even when using a 3 MHz inductor current, ring-like Si melt patterns parallel to the current lines are formed during the FZ process on the surface of the feed rod with a radial size of 1–2 mm (Fig. 1, left). Similar non-uniform melting occurs when a 5 mm thick Si plate is located under the HF inductor (Fig. 1, right). The resulting melt pattern can be used to determine the asymmetry of the inductor currents [3].

It is important to understand the formation of these structures as it is crucial to ensure the continuous and stable melting during the FZ process. The ability to maintain stable growth at relatively low frequencies can be even regarded as a key to grow larger diameter FZ crystals, i.e. larger melting powers can be achieved by lowering the frequency and hence the inductor impedance [4]. Such motivation dictates that a research regarding the inhomogeneous melting during Si HF EM melting is a worthwhile effort.

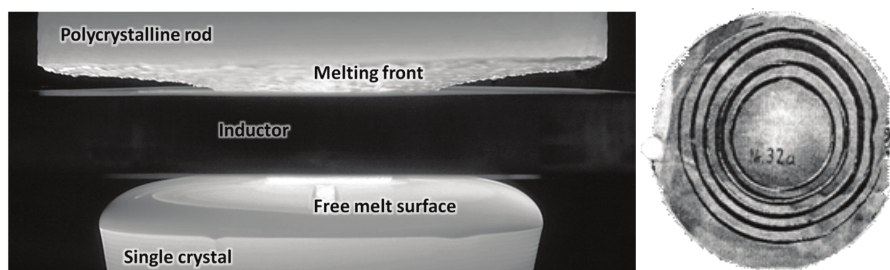


Fig. 1. Left: the inhomogeneous melting front on the feed-rod in the FZ Si growth process [1]. Right: molten rings on a Si plate created by a HF EM inductor [3].

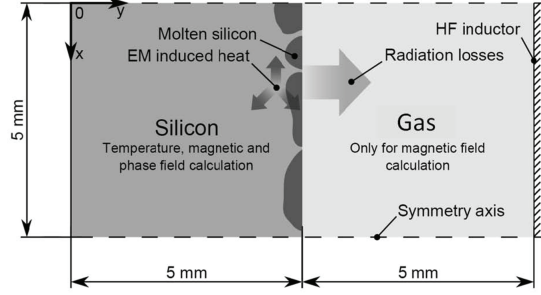


Fig. 2. Schematics of the modelled system. The domain size and the modelled physical processes are depicted.

Melt pattern formation on Si material has been studied previously, e.g., laser beam irradiation on a Si surface creates ridges with a size comparable to the radiation wavelength and orientation determined by the beam polarization [5]. Such a situation arises due to the interference between the incident beam and the scattered radiation from surface imperfections. This example shows that periodic material patterns are a common result of the non-linear system evolution. It is also clear that revealing the driving force of such pattern formation is a valuable contribution to understanding the processes within such non-linear systems.

1. Mathematical model. The previously described problem, arising on the melting front of a polycrystalline Si rod, is studied at a local scale. A two-dimensional (2D) domain of solid Si with dimensions of 5×5 mm and orientation normal to the direction of the electric current is chosen (Fig. 2). It is chosen to be small enough to assume uniform boundary conditions, but sufficiently large for the considered melt patterns to develop. In this region, the temperature field and the phase change are calculated. In order to obtain EM induced heat sources, the magnetic field is calculated in the Si as well as in the gas region between the Si and the inductor surfaces. The possible change of the Si-gas interface after the solid material melting is neglected. It is assumed that the inductor is located at a typical distance of 5 mm from the Si surface. All calculations are made by using a finite difference method implemented within Octave/Matlab environment [6].

The phase field model [7] is used to describe the transient melting-solidification process. A model assumption is made that the phase transition happens within a narrow temperature interval ΔT_S . In such a case, the solid fraction f_c could be modelled as a function of the temperature, as described in [7] (Eq. (1)):

$$f_c = \begin{cases} 0 & \text{if } T > T_0 + \Delta T_S/2 \\ \frac{T_0 + \Delta T_S/2 - T}{\Delta T_S} & \text{if } T \geq T_0 - \Delta T_S/2 \wedge T \leq T_0 + \Delta T_S/2 \\ 1 & \text{if } T < T_0 - \Delta T_S/2 \end{cases} \quad (1)$$

Using this assumption, the transient equation of conductive heat transfer can be written as Eq. (2), where the second term in brackets is associated with the change of enthalpy due to the phase transition:

$$\left(\rho c_p - L \frac{df_c}{dT} \right) \frac{\partial T}{\partial t} = \lambda \Delta T + q_{EM}. \quad (2)$$

The possible motion generated by EM forces and its effect on the heat transfer is neglected. Symmetry or thermal insulation boundary conditions are used on the

Modelling of pattern formation during the melting of silicon by a HF EM field

planes $x = 0$ mm and $x = 5$ mm, a fixed temperature value is used on the inside of the solid domain at $y = 0$ mm, but a radiation condition is used on the surface with gas:

$$\lambda \frac{\partial T}{\partial y} \Big|_{y=5 \text{ mm}} = \varepsilon \sigma_{\text{SB}} T^4. \quad (3)$$

The EM induced heat sources are obtained by calculating the magnetic vector potential (Eq. (4)), which has only one non-zero component A_z normal to the 2D plane in the chosen system geometry:

$$\frac{\partial^2 A_z}{\partial x^2} + \frac{\partial^2 A_z}{\partial y^2} - i\omega\sigma\mu A_z = 0, \quad \sigma_{\text{EM}} = \frac{1}{\sigma} |-i\sigma\omega A_z|^2. \quad (4)$$

Symmetry boundary conditions are used for edges perpendicular to the Si surface at the planes $x = 0$ mm and $x = 5$ mm :

$$\frac{\partial A_z}{\partial x} \Big|_{x=0 \text{ mm}} = 0, \quad \frac{\partial A_z}{\partial x} \Big|_{x=5 \text{ mm}} = 0. \quad (5)$$

It is assumed that deep within the Si bulk (a depth much greater than the skin layer) the magnetic field is zero, thus for the boundary located within the Si bulk A_z is also assumed to be zero. For a boundary, which is associated with the inductor surface, a constant value of k_I is applied:

$$A_z \Big|_{y=0 \text{ mm}} = 0, \quad A_z \Big|_{y=10 \text{ mm}} = k_I. \quad (6)$$

It is varied in order to simulate different inductor currents.

Material properties that are relevant to the developed mathematical model are listed in [8, 9]. These values were obtained in laboratory experiments and are extensively used for mathematical modelling purposes (Table 1).

The electrical conductivities for molten Si $\sigma_m = 1.2 \cdot 10^6$ S/m and solid Si $\sigma_s = 5 \cdot 10^4$ S/m at the melting point should be considered as important parameters with reference to the investigated problem. The emissivity coefficient is modelled as a temperature dependent parameter (Fig. 3, top).

When calculation studies involve large temperature intervals, the temperature dependent electrical conductivity of solid Si is considered as suggested in [10]. It is assumed that the conductivity is determined by two processes: by the generation of conduction electrons and by the presence of dopants in the material (Fig. 3, bottom).

Table 1. Material properties of solid and liquid Si.

| Property | Denotation and value |
|---------------------------------|--|
| melting point | $T_0 = 1685$ K |
| density | $\rho = 2300$ kg/m ³ |
| specific heat capacity | $c_p = 1000$ J/(kg·K) |
| specific volumetric latent heat | $L = 4.14 \cdot 10^9$ J/m ³ |
| thermal conductivity, solid | $\lambda_s = 22$ W/(m·K) |
| thermal conductivity, melt | $\lambda_m = 67$ W/(m·K) |
| electrical conductivity, solid | $\sigma_s = 5 \cdot 10^4$ S/m |
| electrical conductivity, melt | $\sigma_m = 1.2 \cdot 10^6$ S/m |

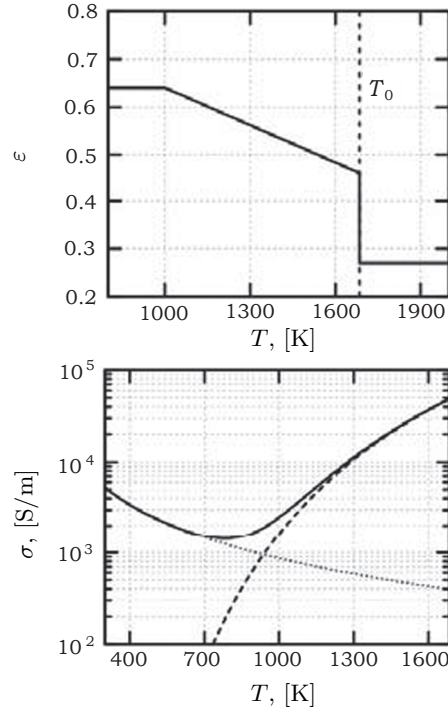


Fig. 3. Top: the modelled Si emissivity coefficient temperature dependence. Bottom: the modelled temperature dependence of solid Si (solid line) as the sum of conduction electron generation (dashed line) and conductivity due to dopants (dotted line).

2. Results and analysis.

2.1. *Basic case.* Calculations were first made with the setup and mesh shown in Fig. 4. The Si domain was divided in 50×50 points with a distance between points of 0.1 mm. Calculations were started from the initial temperature 1645 K, and the temperature at $y = 0$ mm was fixed to this temperature during the whole calculation time. The inductor current was fixed during the calculation time in all studies. This sets the temperature gradient to approx. 80 K/m corresponding to the typical situation in the FZ feed rod. In case of a uniform initial temperature field, a completely uniform melting process takes place with no phase-field distribution variation along the x -direction parallel to the Si surface. The distribution of temperature and EM heat sources along the y -axis is shown in Fig. 5. After 30 ms, a distinct skin-effect with exponential decay of heat sources near the Si surface can be observed. The temperature was rapidly increased also

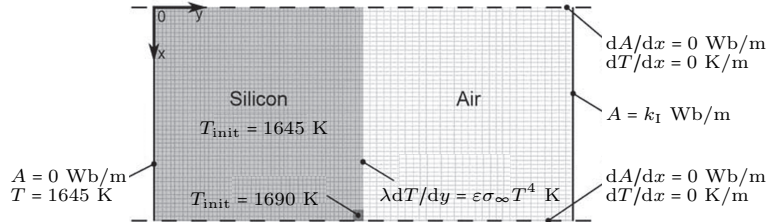


Fig. 4. Schematic of the modelled system. The calculation mesh, initial and boundary conditions are displayed.

Modelling of pattern formation during the melting of silicon by a HF EM field

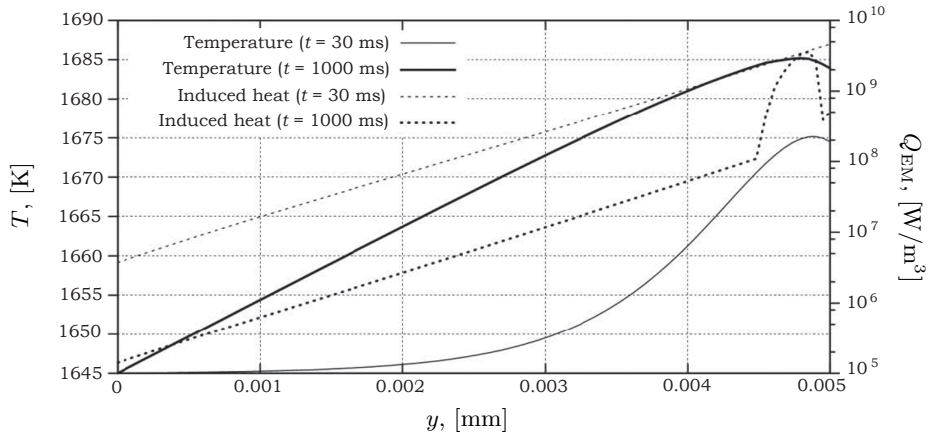


Fig. 5. Distribution of temperature and EM heat sources for two different time moments along the Y axis at $x = 2.5$ mm.

in the vicinity of the Si surface, however, due to thermal radiation; the maximum temperature was reached at a depth of about 0.2 mm. At this position, the Si started to melt, the electric current was concentrated in the molten region with an approximately 25 larger electrical conductivity and the heat sources in solid regions were reduced by about 10 times (see Fig. 5 at 1000 ms). Later, a steady solution was reached, and the duration of the molten zone evolution as well its thickness were determined by the inductor current coefficient k_I .

In order to obtain results featuring the non-uniform melting, an initial temperature field perturbation was used, increasing the temperature of the 0.2×0.2 mm large region at the Si surface to 1690 K (5 K above the melting temperature). In this case, non-symmetric structures developed, and after 20 s stationary structures of the melt regions with a size of about 1.4 mm were obtained for a certain simulated inductor current interval (in Fig. 6, a case with $k_I = 1.2 \cdot 10^{-4}$ Wb/m is shown). This value is in good agreement with typical sizes for the FZ process. The magnetic field lines are bent attempting to increase the skin layer in the solid

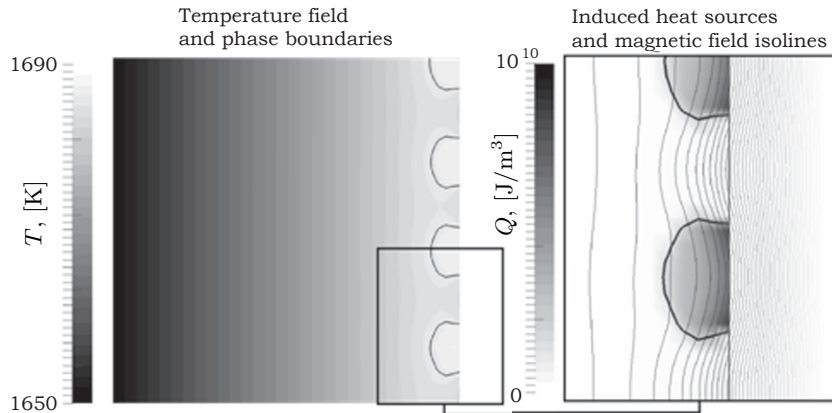


Fig. 6. Calculation results for stationary melt patterns developed starting from initial conditions with a temperature perturbation during a 20 s treatment by the HF EM field (bold lines are phase boundaries).

and decrease the skin layer in the molten material. The electric current and, hence, the induced heat sources are concentrated in molten regions. The emissivity of the melt is almost twice as small as the emissivity of the solid, so the molten regions lose less heat and the solid regions lose more heat, additionally increasing the temperature between them and stabilizing the existence of solid/melt structures along the Si-gas interface.

A distance of 0.1 mm between the mesh points was chosen 3 times smaller than the skin layer depth in the molten Si. To check the influence of the mesh size, it was reduced to 0.05 mm linearly towards the Si-gas interface. The corresponding quasi-stationary result with $k_I = 1.2 \cdot 10^{-4}$ Wb/m after 20 s is shown in Fig. 7, left. If compared to the results on a coarser mesh (Fig. 6), the number of molten regions is the same, but the shape of the molten regions is slightly different, therefore, a finer mesh is used in further calculations.

A study, using different inductor currents (different values of k_I at the inductor boundary) was conducted to determine the range, where the patterns appear. The results of eight cases with a step of $k_I = 0.5 \cdot 10^{-5}$ Wb/m between them showed that the patterns developed between $k_I = 9.5 \cdot 10^{-5}$ Wb/m and $k_I = 11 \cdot 10^{-5}$ Wb/m. For larger inductor currents, the structures were larger, i.e. there were less melt regions. With a smaller inductor current, the surface was solid, and with a larger currents – molten.

Another method to initiate the non uniform melting and development of melt-solid patterns is the application of a non-uniform inductor current. Similar steady state patterns were obtained when a non-uniform (linear distribution with a 2–10% change over 5 mm length) vector potential boundary condition at the inductor surface was used. Fig. 7 (middle and right) shows melt-solid patterns at the 20 s time moment after the start of the simulation from a constant temperature. The figure in the center shows the case with 2% inhomogeneity of the vector potential and on the right side – with 4% inhomogeneity. There are four melt regions with 2% inhomogeneity, but 3.5 melt regions with 4% inhomogeneity. Obviously, the distance between the regions depends on the structure formation process.

2.2. Analysis of integral heat sources. The amount of molten Si at the melting front determines the induced heat at the given inductor current. Usually the presence of a thin melt layer on the feed rod is modelled indirectly in a global heat transfer model, by using assumptions on the total induced heat depending on the expected thickness of this layer [11]. This approach does not consider non-uniformities of the melting interface calculated in section 3.1. By numerically



Fig. 7. Temperature field and phase boundaries (black lines) developed under non-uniform initial conditions (left) and with a uniform magnetic vector potential at the inductor surface. Variation of the magnetic vector potential is 2% (middle) and 4% (right).

Table 2. Total induced heat QEM within the modelled Si domain for different phase distributions and fixed inductor current. The ratio of the induced heat ξ is compared to a uniform melt case.

| Type of phase distribution | Q_{EM} , [kW/m] | ξ |
|--|-------------------|-------|
| uniformly solid | 14.80 | 5.07 |
| homogenous melt layer (0.25 mm) | 3.39 | 1.16 |
| melt patterns (volume as 0.25 mm melt layer) | 4.74 | 1.63 |
| uniformly liquid | 2.92 | 1.00 |

integrating the obtained induced heat source distribution, it is possible to determine the effect of the melt structure on the total induced heat. Table 2 lists the integral heat sources for cases with solid material (uniformly solid), a homogeneous melt layer with a thickness of 0.25 mm, melt-solid structures (Fig. 7, left) with the amount of melt corresponding to the 0.25 mm homogeneous melt layer and thick melt layer (uniformly liquid). It can be concluded that the melt distribution within the localized regions ensures a by about 40% larger induced heat than in the case of the same melt volume creating the homogenous melt layer. Considering this difference, the precision of global FZ models can be increased.

2.3. *Studies with varied material properties.* Further studies considered different material properties to locate the determinative parameters which ensure the melt pattern formation and influence the arrangement of these patterns. Varied parameters are the electrical conductivity of solid Si, the frequency of EM field and the emissivity coefficient of the melt.

By applying an equal fixed value of 0.64 for the emission coefficient of both the melt and the solid, it was observed that the pattern formation still occurred (see Fig. 8). However, in this case, a solid Si layer was formed on the top of the melt regions due to comparatively larger radiative losses from the surface. This proves that different emissivity properties of solid and liquid Si are supporting, but not crucial for the observed phenomena.

The variation of the electrical conductivity and frequency changes the distance between the molten regions. Both changes can be analyzed in the context of skin-layer depth (where is the frequency, is the electrical conductivity, but is the magnetic constant). The distance between the centers of the first two molten regions, starting from the place of initial inhomogeneity, is analyzed, as it was

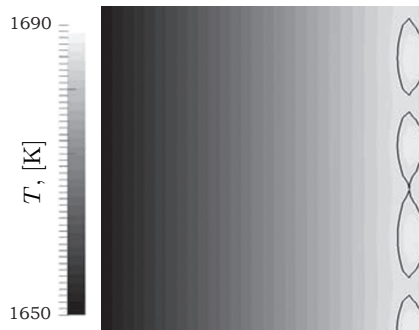


Fig. 8. Temperature field and phase boundaries (black lines) in the case with one equal emission coefficient for melt and solid material.

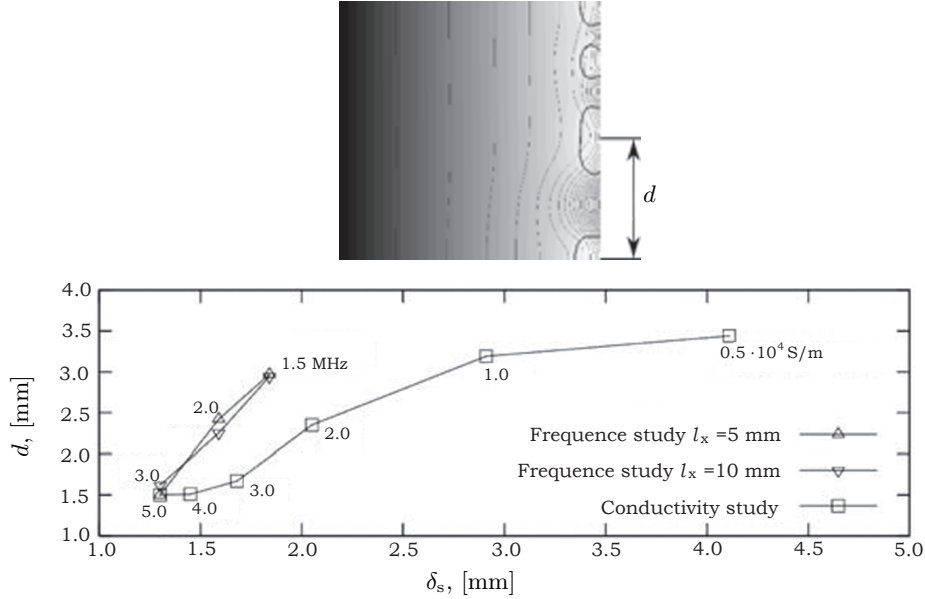


Fig. 9. Left: the calculated temperature field, phase boundary (thick black line) and magnetic field at a reduced solid electrical conductivity of $2 \cdot 10^4$ S/m. Right: the melt region size d as a function of the skin-depth in solid Si for calculations with various frequencies (triangular data points) and solid Si electrical conductivities (rectangular data points).

shown for the case with an electrical conductivity of 2104 S/m in Fig. 9, left. The distance d as a function of the skin-layer depth in solid material is shown in Fig. 9, right. Decreasing the conductivity of the solid material increases the distance between the molten regions, and decreasing the frequency does the same. However, with the same skin-layer depth, the effect is stronger in the case of decreased frequency, as in this case the skin layer in molten Si decreases as well. Note that the spatial pattern remained unchanged if a twice as long domain size l_x was used for calculations (compare lines with triangle and upside down triangle symbols in Fig. 9, right).

2.4. Case with different thermal conditions. To simulate the molten lines formed on the 5 mm thick Si plate under the HF EM inductor (Fig. 1, right), calculations were performed using the radiation boundary condition also on the left side of the Si domain. The calculation geometry for the EM field was extended by a gas domain at the left side of Si. Additionally, an initial temperature of 300 K was used in the domain (with a 45 K perturbation at the corner) to simulate the effects of extremely varying electrical conductivity (as in Fig. 3, right). In this case, stationary melt patterns were not obtained, and the patterns developed after 3.5 s disappeared after 16 s (Fig. 10). Additionally, the distance between the observed melt regions was larger than in the case illustrated in Fig. 7, hence, the thermal gradient in Si influences the development of patterns as well.

3. Conclusions. The present work demonstrates that the melt pattern formation during the inductive melting of silicon is determined by the EM field interaction with a two-phase environment with different electrical conductivities. The non-uniform initial temperature or the non-uniform inductor current is a prerequisite for the development of these patterns. The smaller emissivity of the melt supports the development of the patterns, but is not crucial. The characteristic

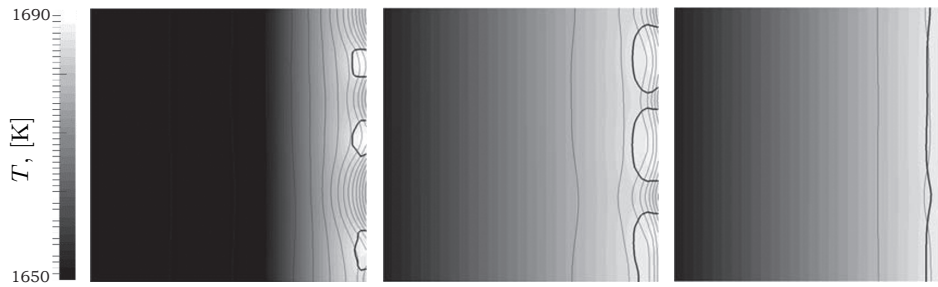


Fig. 10. The calculated temperature field, phase boundary (thick black line) and magnetic field (thin black lines). From left to right: time instances of 3.5, 8.0 and 16.0 seconds.

size of the patterns was shown to be around 1.4 mm, which corresponds well to the observed situation in the floating-zone furnaces. Wider patterns were obtained at lower solid Si electrical conductivities, which also corresponds qualitatively to the observations [3]. The size of the patterns is related to the skin-layer depth in the solid and molten material, but also depends on thermal boundary conditions.

Acknowledgements.

This work was supported by the European Regional Development Fund, project contract no. 2013/0051/2DP/2.1.1.1.0/13/APIA/VIAA/009.

REFERENCES

- [1] T. DUFFAR. *Crystal Growth Processes Based on Capillarity: Czochralski, Floating Zone, Shaping and Crucible Techniques* (Wiley-Blackwell, 2010).
- [2] W. WNSCHER, A. LUDGE AND H. RIEMANN. Crucible-free pulling of germanium crystals. *J. Crystal Growth*, vol. 318 (2011), no. 1, pp. 1039–1042.
- [3] H. RIEMANN, A. LUDGE, K. BOTTCHE, H.J. ROST, B. HALLMANN, W. SCHRODER, W. HENSEL AND B. SCHLEUSENER.. Silicon floating zone process: numerical modeling of RF field, heat transfer, thermal stress, and experimental proof for 4 inch crystals. *J. The Electrochemical Society*, vol. 142 (1995), no. 3, pp. 1007–1014.
- [4] R. MENZEL. *Growth Conditions for Large Diameter FZ Si Single Crystals* (PhD. Thesis at the Technische Universitt Berlin, 2013).
- [5] J.F. YOUNG, J.S. PRESTON, H.M. VAN DRIEL AND J.E. SIPE. Laser-induced periodic surface structure. II. Experiments on Ge, Si, Al, and brass. *Phys. Rev. B*, vol. 27 (1983), no. 2, pp. 1155–1172.
- [6] J.W. EATON, D. BATEMAN, AND S. HAUBERG. *GNU Octave Manual Version 3* (Network Theory Limited, 2008).
- [7] I. STEINBACH, M. APEL, T. RETTELBACH AND D. FRANKE. Numerical simulations for silicon crystallization processes – examples from ingot and ribbon casting. *Solar Energy Materials and Solar Cells*, vol. 72 (2002), no. 1-4 pp. 59–68.
- [8] A. MUHLBAUER, A. MUIZNIEKS, J. VIRBULIS, A. LUDGE AND H. RIEMANN. Interface shape, heat transfer and fluid flow in the floating zone growth of large

silicon crystals with the needle-eye technique. *J. Crystal Growth*, vol. 151 (1995), no. 1-2, pp. 66–79.

- [9] A. SABANSKIS, K. BERGFELDS, A. MUIZNIEKS, T. SCHRCK AND A. KRAUZE. Crystal shape 2D modeling for transient CZ silicon crystal growth. *J. Crystal Growth*, vol. 377 (2013), pp. 9–16.
- [10] C. KITTEL. *Introduction to Solid State Physics* (8th ed., Wiley, 2005).
- [11] G. RATNIEKS. *Modelling of the Floating Zone Growth of Silicon Single Crystals with a Diameter up to 8 Inches* (PhD thesis, University of Latvia, 2007).

Received 31.01.2015